# Effect of Ti compositions for efficiency enhancement of $CaTiO_3$:Er,Ni broadband-sensitive upconverters

Hom Nath Luitel*, Shintaro Mizuno, Takamasa Nonaka, Toshihiko Tani, Yasuhiko Takeda*
Toyota Central Research and Development Laboratories, Nagakute, Aichi 480-1192, Japan

*Corresponding Authors:
E-mail: mehomnath@yahoo.com (H.N. Luitel),
takeda@mosk.tytlabs.co.jp (Y. Takeda)
Tel.: +81 561 717306; Fax: +81 561 636137

**Electronic supplementary information:**

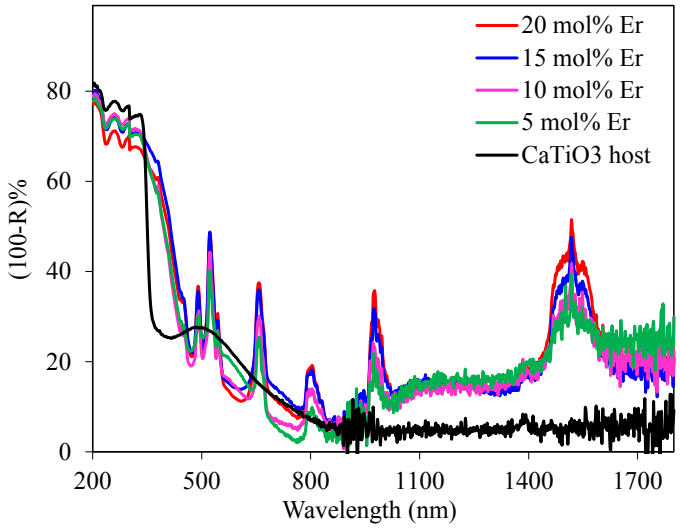


Fig. S1 Absorption spectra of the $CaTiO_3$:0.2 mol% Ni codoped with different mol% of Er.

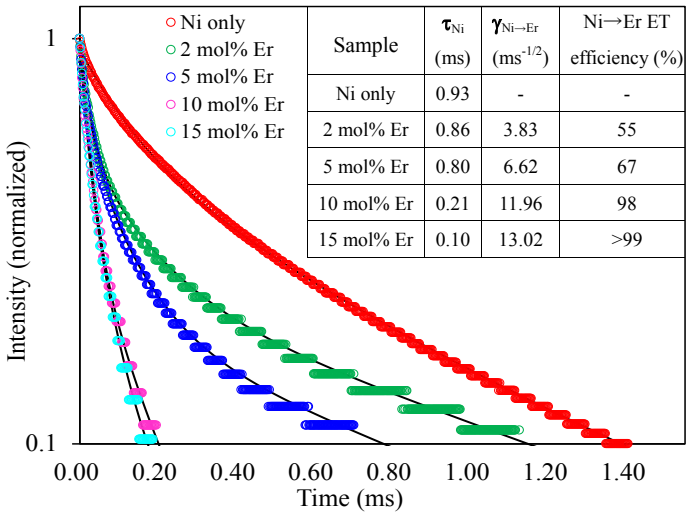


| Sample | $\tau_{Ni}$ (ms) | $\gamma_{Ni\rightarrow Er}$ ($ms^{-1/2}$) | Ni→Er ET efficiency (%) |
|---|---|---|---|
| Ni only | 0.93 | - | - |
| 2 mol% Er | 0.86 | 3.83 | 55 |
| 5 mol% Er | 0.80 | 6.62 | 67 |
| 10 mol% Er | 0.21 | 11.96 | 98 |
| 15 mol% Er | 0.10 | 13.02 | >99 |

Fig. S2 Time decay profiles of the $Ni^{2+}$ emission at 1400 nm ($^3T_2 \rightarrow {}^3A_2$ transition) with variable $Er^{3+}$ doping concentrations (excited at 1180 nm).Solid black lines are the results of fitting using the equations mentioned below. Inset shows the comparison of decay time, Ni→Er ET extents and Ni→Er ET efficiencies.

The time decay profiles of the $Ni^{2+}$ emission at 1400 nm for the Ni-only doped sample was compared with those for the Er, Ni codoped sample. The measured time-dependent intensity of the Ni-only doped sample was fitted by a bi-exponential function,

$$I_{\text{Ni-only}}(t) = a_{\text{Ni}} \exp\left[-t/\tau_{\text{Ni}}^{(1)}\right] + b_{\text{Ni}} \exp\left[-t/\tau_{\text{Ni}}^{(2)}\right], \quad \ldots\ldots\ldots (1)$$

and the $Ni^{2+}$ lifetime $\tau_{\text{Ni}}$ was determined by the equation (2) below for the Ni-only doped samples,

$$\tau_{\text{Ni}} = (a_{\text{Ni}}\, \tau_{\text{Ni}}^{(1)2} + b_{\text{Ni}}\, \tau_{\text{Ni}}^{(2)2}) / (a_{\text{Ni}}\, \tau_{\text{Ni}}^{(1)} + b_{\text{Ni}}\, \tau_{\text{Ni}}^{(2)}), \quad \ldots\ldots\ldots\ldots (2)$$

The $\tau_{\text{Ni}}$ value of the $CaTiO_3$:0.2 mol% $Ni^{2+}$ sample is 0.93 ms, which is comparable with the values previously reported for other oxide host materials.[1-6]

By introducing the $Er^{3+}$ acceptors, the $Ni^{2+}$ emission intensity declines rapidly because of the energy transfer from the $Ni^{2+}$ donors to the $Er^{3+}$ acceptors. The life time of Ni-emissions in the Ni, Er codoped samples ($\tau_{\text{Ni,Er}}$ value) were also estimated (inset of Fig. S2), which is equals to the time when Ni-emission intensity decreased to 1/e of the initial intensity. It showed that with increasing $Er^{3+}$ concentration $Ni^{2+}$ emission life time reduced sharply. The impact of the energy transfer on the time-dependent emission intensity of the $Ni^{2+}$ donors is expressed by an exponential function $\exp\left[-w_{\text{Ni}\to\text{Er}}\, t\right]$ when energy migration among the donors are significant, [7-10] whereas it is described as $\exp\left[-\gamma_{\text{Ni}\to\text{Er}}\sqrt{t}\right]$ for negligibly weak migration [10-12]. The experimental data were well fitted by the latter better than the former, *i.e.*,

$$I_{\text{Ni,Er}}(t) = \exp\left[-\gamma_{\text{Ni}\to\text{Er}}\sqrt{t}\right] I_{\text{Ni-only}}(t), \quad \ldots\ldots\ldots\ldots\ldots\ldots (3)$$

using a fitting parameter $\gamma_{\text{Ni}\to\text{Er}}$ with the previously determined $I_{\text{Ni-only}}(t)$. This is consistent with the facts that the Ni concentration was quite low (0.2 mol%) and the energy transfer was completed rapidly within sub-milliseconds. The energy transfer efficiency $\eta_{\text{Ni}\to\text{Er}}$ was derived as follows,

$$\eta_{\text{Ni}\to\text{Er}} = 1 - \int_0^\infty dt\, I_{\text{Ni, Er}}(t) \Big/ \int_0^\infty dt'\, I_{\text{Ni-only}}(t'), \quad \ldots\ldots\ldots\ldots (4)$$

using the two functions in equations (1) and (3). The $\eta_{\text{Ni}\to\text{Er}}$ increased with the Er concentration reaching near to unity above 10 mol% Er. It confirmed that almost all the energy absorbed by the $Ni^{2+}$ get transferred to the $Er^{3+}$ emission centers. This value is higher compared to the previously reported $CaZrO_3$:Er,Ni upconverter where ~86% energy transfer efficiency was observed even at high Er concentrations.[13]

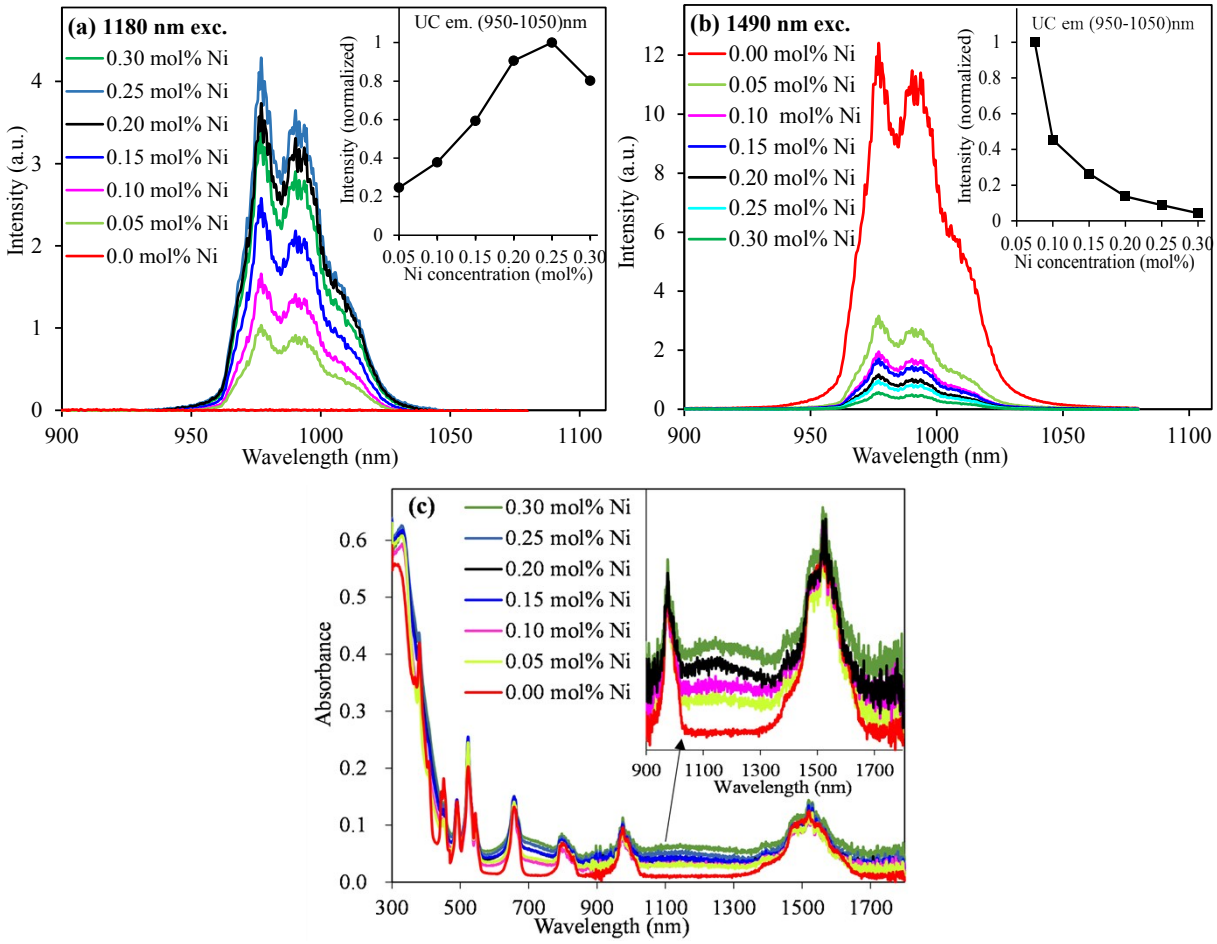


Fig. S3 UC emission spectra of the $CaTi_{0.9}O_3$:15 mol% Er codoped with different mol% of Ni excited at (a) 1180 nm, (b) 1490 nm, and (c) absorption spectra. Inset in Fig. (c) shows the enlarged view of selected area.

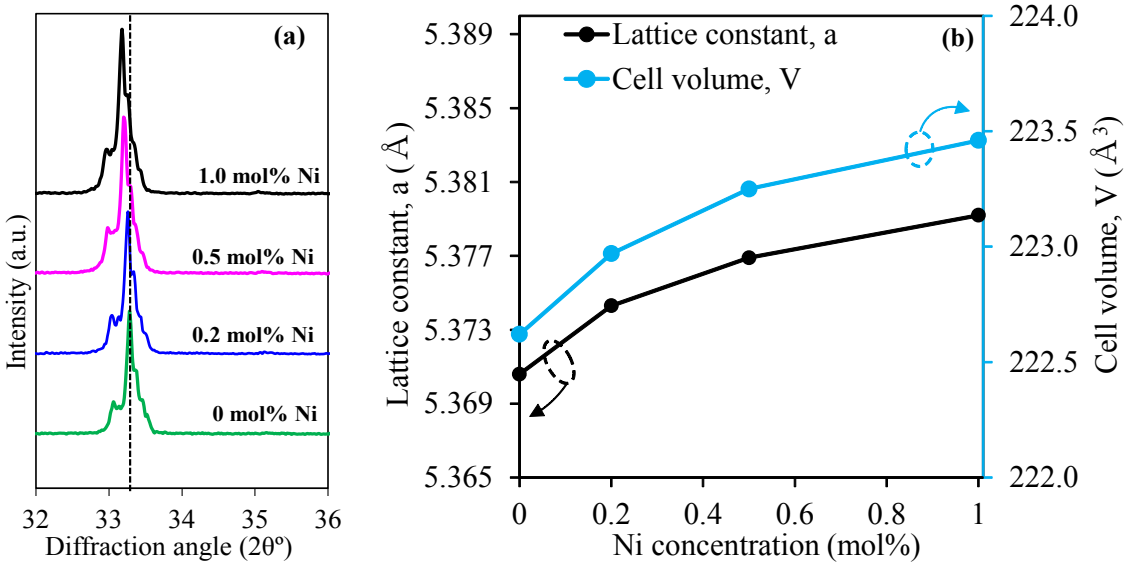


Fig. S4 Effects of the NiO doping concentrations on (a) the XRD peaks positions of $CaTiO_3$ phase and (b) variation of lattice parameters.

In the $CaTiO_3$ host, addition of $Er^{3+}$ (ionic size ≈ 1.06 Å) and $Ni^{2+}$ (ionic size ≈ 0.69Å) ions are expected to substitute the $Ca^{2+}$ (~1.12Å) and $Ti^{4+}$ (~0.605Å) sites because of their comparable ionic radii.[14] Substitution of $Ca^{2+}$ sites

with $Er^{3+}$ ions has been confirmed in the $CaZrO_3$:Er,Ni upconverters.[13] Here substitution of $Ti^{4+}$ with the $Ni^{2+}$ ions was confirmed from the XRD data of the various moles of Ni-substituted samples as shown in Fig. S4, where increased lattice parameters and cell volume was observed when bigger $Ni^{2+}$ ions substitutes the smaller $Ti^{4+}$ ions. If the $Ca^{2+}$ ions were substituted by the $Ni^{2+}$ ions (quite smaller compared to the $Ca^{2+}$ ions), drastic decrease in cell volume and lattice parameters would be expected. The increased cell parameters further suggests that the Ni ions stabilize as $Ni^{2+}$ (ionic size ≈ 0.69Å) not $Ni^{3+}$ (ionic size ≈ 0.59Å). If Ni ions would stabilize as $Ni^{3+}$ cell parameters should remain constant due to same size of $Ni^{3+}$ to that of $Ti^{4+}$.

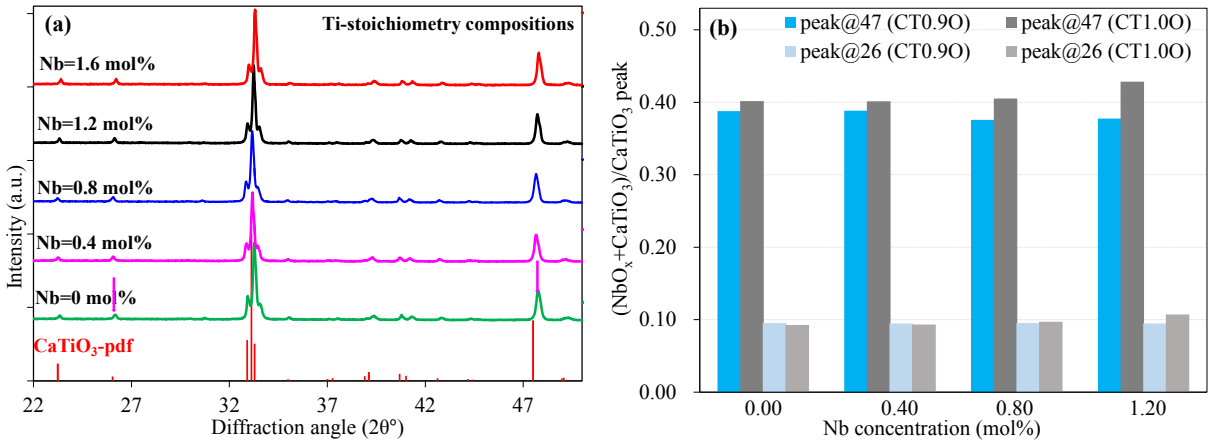


Fig. S5 Effect of the $Nb_2O_5$ concentration on (a) the XRD peaks of $CaTiO_3$ phase and (b) increased peak intensity at the $NbO_x$ peaks positions at 26.2 and 47.6 degree compared to the $CaTiO_3$ peak intensity at 33 degree, where $NbO_x$ peak was absent.

$NbO_x$ peaks at 2Θ equals 26.2 and 47.6 degree, which overlap with the $CaTiO_3$ host peaks, remarkably increased with the Nb doping concentrations at and above 1.2 mol% indicating segregation of the $NbO_x$ phase in the Ti-stoichiometric samples ($CT_{1.0}O$), whereas they were almost unchanged for the Ti-deficit ($CT_{0.9}O$) samples up to 1.2 mol% Nb doping.

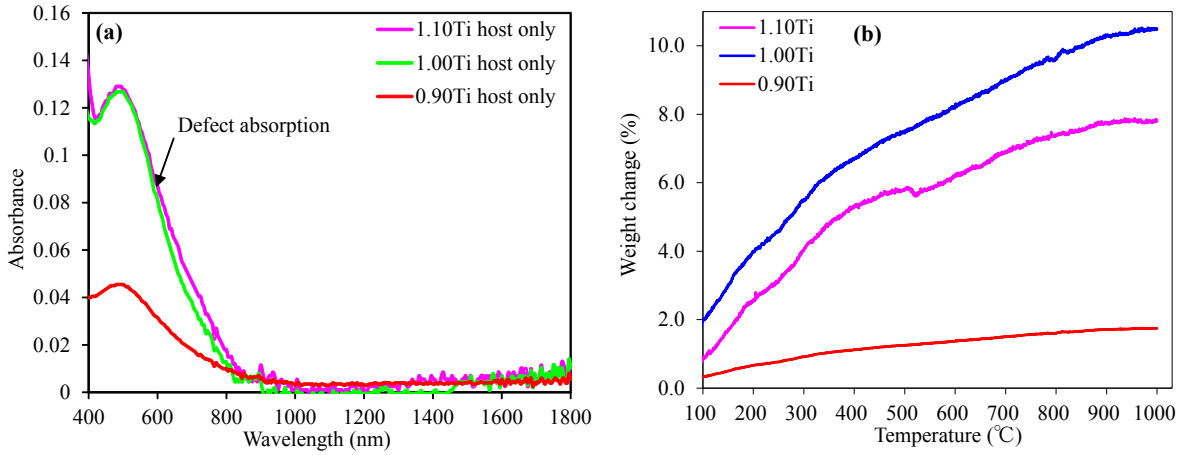


Fig. S6 (a) Absorption spectra of the $CaTiO_3$ host with different Ti-compositions, and (b) weight gain of the respective samples with rising of temperature in air flow.

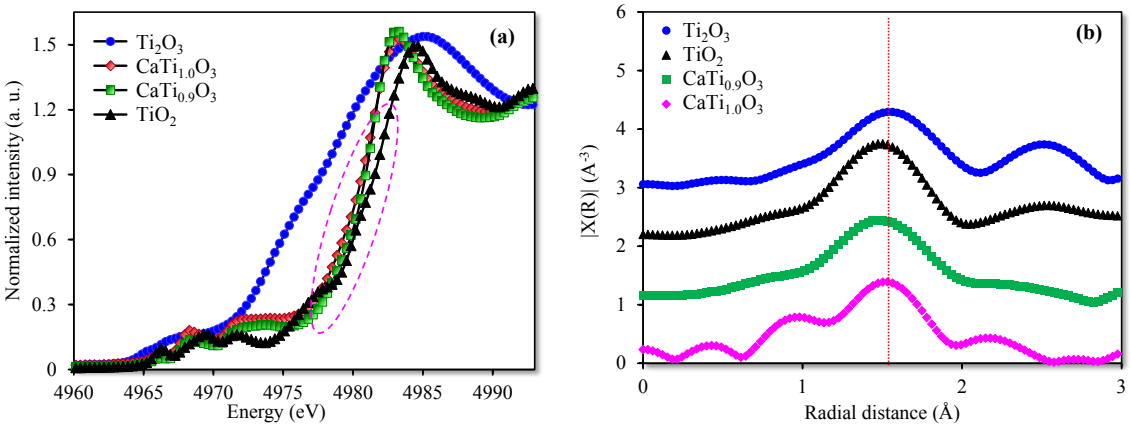


Fig. S7 (a) XANES spectra of $TiO_2$, $Ti_2O_3$, $CaTi_{1.0}O_3$, $CaTi_{0.9}O_3$ and (b) bonding length of Ti-O bond in compounds mentioned in (a).

The X-ray absorption near edge structure (XANES) spectra of the Ti-deficit and Ti-stoichiometric samples compared with the standard $TiO_2$ and $Ti_2O_3$ samples were measured to identify the valence of Ti in the $CaTiO_3$ samples.[15,16] The absorption edge of the Titanium atoms in both of the Ti-defict and Ti-stoichiometric samples are very close to that of the $TiO_2$ standard sample (marked by the dotted circle in Fig. S7 (a)) confirming that the Ti-atoms existed as $Ti^{4+}$ ions irrespective of small variation in Ti-compositions. We also tried to figure out the valance of the nickel ions in the $CaTiO_3$:Er,Ni upconverters comparing with the standard $Ni^{2+}$ and $Ni^{3+}$ samples using fluorescence X-ray absorption fine structures (XAFS), however, due to close absorption edge energies of the Er-L3 edge and Ni-K edge and very small doping concentrations of the Ni (0.2 mol%) compared to Er (15 mol%), it was not possible to extract Ni contribution in the Er, Ni codoped samples.

We also determined the Ti-O bond length from Extended X-ray Absorption Fine structures (EXAFS) for those samples and compared with each other and the results are presented in Fig. S7(b). The Ti-O bond becomes shorter for the Ti-deficit ($CaTi_{0.9}O_3$) sample compared to in the Ti-stoichiometric ($CaTi_{1.0}O_3$) sample. It suggests that the Ti-O bonds are stronger in the Ti-deficit compositions compared to that in the Ti-stoichiometric compositions.

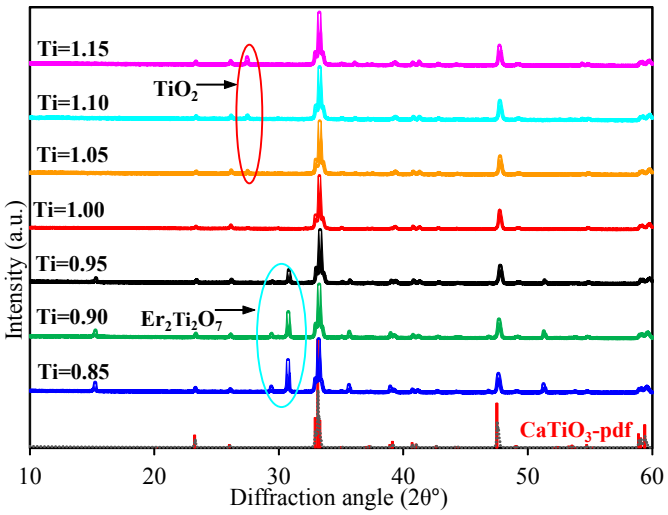


Fig. S8 XRD patterns of $CaTiO_3$:15%Er, 15% Li, 0.2% Ni, 0.4% Nb with various Ti-compositions.

It is obvious that above the solid solubility limit, added $TiO_2$ remained as unreacted phase, clearly observed in the Ti-excess compositions, which is remarkably increased at 0.15 mole Ti-excess composition. On the other hand,

in the Ti-deficit compositions, $Er_2Ti_2O_7$ phase was detected and its amount gradually increased with the increasing Ti-deficiency. $Er_2Ti_2O_7$ phase is a prototype of the $Ca_2Nb_2O_7$ pyrochlore phase and consume lower equivalent of $Ti^{4+}$ ions. Thus, to compensate the Ti-deficiency, more and more $Er_2Ti_2O_7$ phase was formed. There is no change in the B-site cations coordination in both perovskite structure and pyrochlore structures and form regular $TiO_6$ octahedra in both cases.

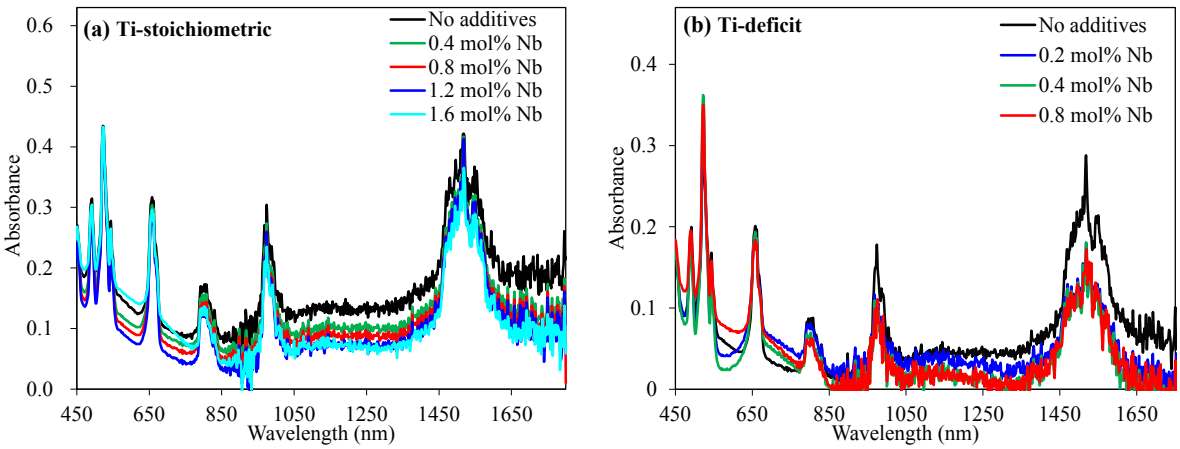


Fig. S9 Absorption spectra of (a) Ti-stoichiometric and (b) Ti-deficit $CaTiO_3$:15 mol% Er, 0.2 mol% Ni codoped with various concentrations of $Nb^{5+}$ as a charge compensator.

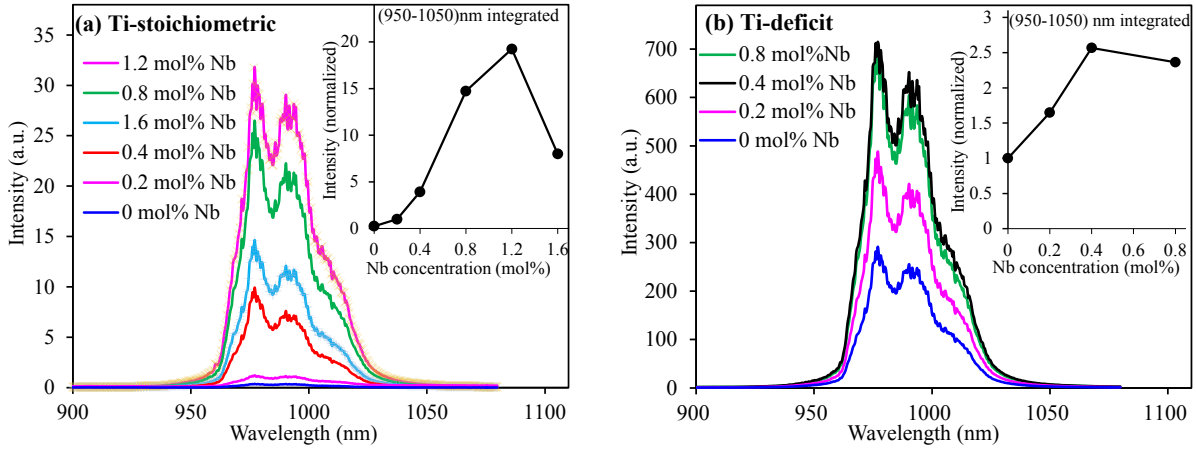


Fig. S10 UC emission spectra of the $CaTiO_3$:15 mol% Er, 0.2 mol% Ni codoped with various concentrations of $Nb^{5+}$ as a charge compensator. Inset figures show the integrated UC intensity variation with the $Nb^{5+}$ concentrations.

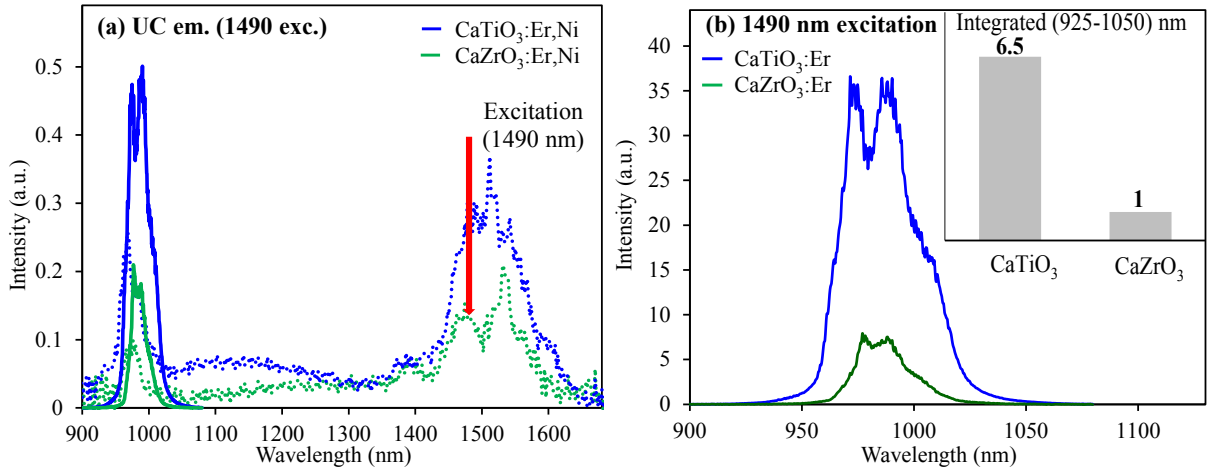


Fig. S11 (a) Comparison of the absorbance in the NIR range for the $CaTiO_3$:15 mol% Er, 0.2 mol% Ni codoped with the $CaZrO_3$:15 mol% Er, 0.2 mol% Ni and corresponding UC emission spectra excited at 1490 nm. The dotted lines represent the absorption spectra while the solid lines are the UC emission spectra. (b) Comparison of the UC emissions intensities for the Er-only doped $CaTiO_3$ and $CaZrO_3$ upconverters exhibiting pronounced emission in more distorted $CaTiO_3$ host.

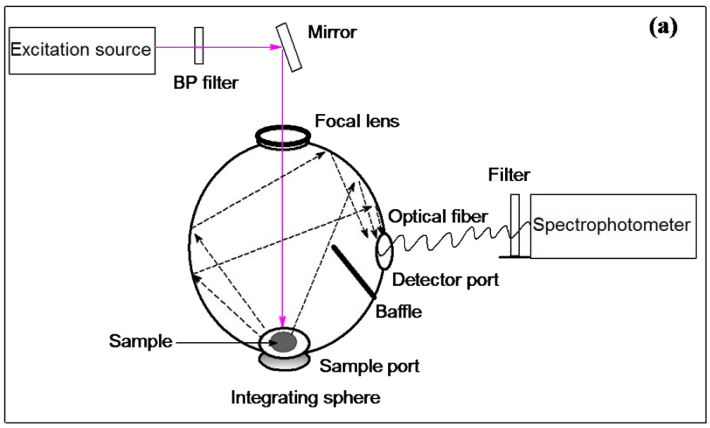


Fig. S12 Experimental setup for the internal quantum yield measurements of the UC emission.

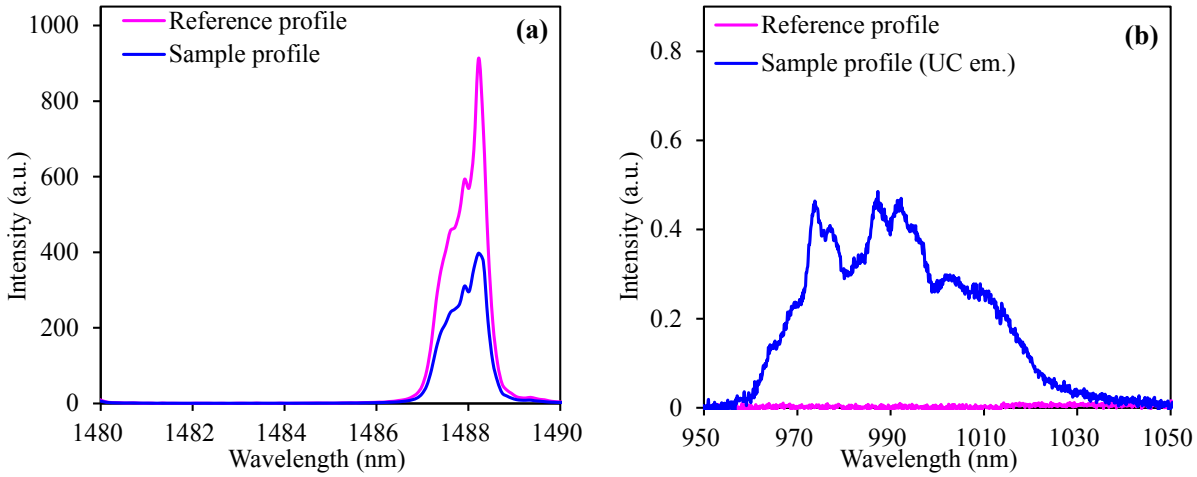


Fig. S13 (a) Reflected laser emission at 1488 nm for a reference cell compared with the $CaTiO_3$:Er,Ni sample and (b) UC emission profile at 950-1050 nm for a $CaTiO_3$:Er,Ni sample compared with the reference cell.

Internal quantum yiled (QY) is defined as the ratio of the number of photons emitted to the absorbed ones. Thus, the number of photons emitted and absorbed should be evaluated precisely to determine the QY of upconverters. An integrating sphere conntected with a spectrophotometer is generally employed to evaluate the photons numbers participated in the UC process. The sketch of the the QY measurement setup is presented in Fig. S12. A blank sample holder (quartz glass) is located at the bottom of the integrating sphere. Excitation light of 1490 nm were incident from the entrance port to be precisely focused on the sample holder. A convergent lens was used to focus the excitation light from the laser diodes. The spectroscopic data were recorded and corrected with the spectral response of the integrating sphere and spectrophotometer. Then, the sample holder was replaced with the sample using the identical holder. The spectra were again recorded and similarly corrected. Then, the QY value (η) is derived using the following equation.[17,18]

$$\eta = \frac{number\ of\ photons\ emitted}{number\ of\ photons\ absorbed} = \frac{I\ (sample\ UC)}{E\ (reference) - E\ (sample)} \quad \text{..... (5)}$$

Where, *I*(sample UC) is the integrated UC emission photon number of the sample, *E*(reference) and *E*(sample) are the integrated photon numbers of the excitation laser light reflected (not absorbed) by the reference holder and sample, respectively. Typical experimental resluts are presented in Fig. S13. For the optimized sample, namely $CaTi_{0.9}O_3$:15% Er, 0.2% Ni, 15%Li, 0.4%Nb, the UC QY was estimated to be ~2.53% under the 1490 nm laser of 1000 W/m$^2$ irradiation whereas it was only ~0.86% for the 1180 nm laser irradiation of very similar power density. Less than 10% error arising from the reabsorption of the emitted photons at the excitation wavelength of 1490 nm was possible because it was omitted during the QY determination due to neglegible emission peak intensity.

## References

1. Y. Takeda, S. Mizuno, H. N. Luitel, K. Yamanaka and T. Tani, *Journal of Applied Physics*, 2016, **120**, 073102.
2. H. N. Luitel, S. Mizuno, T. Tani and Y. Takeda, *Optical Materials*, 2017, **64**, 314-322.

3. G. Dong, M. Liang, H. Qin, G. Chai, X. Zhang, Z. Ma, M. Peng and J. Qiu, *Phys. Chem. Chem. Phys.*, 2012, **14**, 13594.
4. B. Wu, J. Qiu, E. Wu and H. Zeng, *Optical Materials*, 2013, **35**, 983.
5. S. Ye, Y. Zhang, H. He, J. Qiu and G. Dong, *Journal of Materials Chemistry C*, 2015, **3**, 2886-2896.
6. G. Bai, Y. Zhang and J. Hao, *Journal of Materials Chemistry C*, 2014, **2**, 4631.
7. T. Förster, *Annalen der Physik*, 1948, **437**, 55-75.
8. D. L. Dexter, *J. Chem. Phys.*, 1953, **21**, 836.
9. M. Inokuti and F. Hirayama, *Journal of Chemical Physics*, 1965, **43**, 1978.
10. Y. Takeda, S. Mizuno, H. N. Luitel and K. Yamanaka, *Applied Physics Express*, 2016, **9**, 112402.
11. A. I. Burshteĭn, *Sov. Phys. JETP* 1972, **35**, 882.
12. J. A. Caird, A. J. Ramponi and P. R. Staver, *Journal of Optical Society of America B*, 1991, **7**, 1391-1403.
13. H. N. Luitel, S. Mizuno, T. Tani and Y. Takeda, *RSC Adv.*, 2016, **6**, 55499-55506.
14. http://abulafia.mt.ic.ac.uk/shannon/ptable.php).
15. T. Nonaka, K. Dohmae, Y. Hayashi, T. Araki, S. Yamaguchi, Y. Nagai, Y. Hirose, T. Tanaka, H. Kitamura, T. Uruga, H. Yamazaki, H. Yumoto, H. Ohashi and S. Goto, *AIP Conf. Proc.*, 2016, **1741**, 030043.
16. T. Nonaka, K. Dohmae, T. Araki, Y. Hayashi, S. Yamaguchi, Y. Hirose, Y. Nagai, T. Uruga, H. Yamazaki, T. Mochizuki, H. Tanida and S. Goto, *Review of Scientific Instruments*, 2012, **83**, 083112.
17. N. C. Dyck, F. C. J. M. van-Veggel and G. P. Demopoulos, *ACS Materials Interface*, 2013, **5**, 11661-11667.
18. I. Etchart, PhD Dissertation, University of Cambridge 2010.